Controlled Rupture of Magnetic Polyelectrolyte Microcapsules for Drug Delivery

Shang-Hsiu Hu, Chia-Hui Tsai, Chen-Fu Liao, Dean-Mo Liu,* and San-Yuan Chen*

Department of Materials Sciences and Engineering, National Chiao Tung University, Hsinchu, Taiwan, 300, Republic of China

Received April 11, 2008. Revised Manuscript Received July 11, 2008

In this study, a magnetic-sensitive microcapsule was prepared using Fe_3O_4/poly(allylamine) (Fe_3O_4/PAH) polyelectrolyte to construct the shell. Structural integrity, microstructural evolution, and corresponding release behaviors of fluorescence dyes and doxorubicin were systematically investigated. Experimental observations showed that the presence of the magnetic nanoparticles in the shell structure allowed the shell structure to evolve from nanocavity development to final rupture of the shell under a given magnetic stimulus of different time durations. Such a microstructural evolution of the magnetic sensitive shell structure explained a corresponding variation of the drug release profile, from relatively slow release to burst-like behavior at different stages of stimulus. It has proposed that the presence of magnetic nanoparticles produced heat, due to magnetic energy dissipation (as Brown and Néel relaxations), and mechanical vibration and motion that induced stress development in the thin shell. Both mechanisms significantly accelerated the relaxation of the shell structure, causing such a microstructural evolution. With such a controllable microstructural evolution of the magnetic-sensitive shell structure, active substances can be well-regulated in a manageable manner with a designable profile according to the time duration under magnetic field. A cell culture study also indicated that the magnetic-sensitive microcapsules allowed a rapid uptake by the A549 cell line, a cancerous cell line, suggesting that the magnetic-sensitive microcapsule with controllable rupturing behavior of the shell offers a potential and effective drug carrier for anticancer applications.

Introductions

Microcapsules have received great interest for drug delivery and biomedical applications, as they provide numerous advantages, such as high payloads of active substances and physical and chemical versatilities of the capsule's shells that can be engineered to facilitate specific applications.[1−6] The microcapsules exhibiting small size, large inner volume, and high total surface area develop via layer-by-layer (LbL) assembly on the nano- or microcores, which can construct thin layers through alternative adsorption of oppositely charged ions, biomolecules, and/or nanoparticles.[7−13] Many studies used organic or inorganic cores to carry drugs and design suitable shells to deliver active substances.[14−17] By modifying the surface of capsules with specific agents such as antibodies or proteins, a targeting delivery to specific site of diseases for therapeutic purpose can be achieved. Such a site-specific delivery has been well-elaborated in medical and pharmaceutical fields, where higher drug-loading efficiency and lower toxicity can be achieved simultaneously.

Stimuli-responsive microcapsules permit tunable permeability for therapeutic molecules with a controllable release profile based on a predesigned mechanism under a given environmental stimulus. The release rate of therapeutic molecules from microcapsules is usually controlled by the diffusion rate of the molecules across the microcapsule shell. On this basis, a fast response of the shell structure to environmental stimuli may be designable. Modern environmental stimuli-responsive microcapsules have been reported in response to specific stimuli, such as temperature,[19−21] pH,[22−28] light,[29,30] external electric field,[31] ultrasound,[32,33] and glucose,[34] and these "smart" microcapsules continue to receive increasingly attentions.

* Corresponding authors. Tel: 8863-5712121, ext. 31818. Fax: 8863-5725490. E-mail: sanyuanchen@mail.nctu.edu.tw (S.Y.C.), deanmo_liu@yahoo.ca (D.M.L.).

(1) Bellomo, E. G.; Wyrsta, M. D.; Pakstis, L.; Pochan, D. J. *Nat. Mater.* **2004**, *3*, 244–248.
(2) Wygladacz, K.; Ye, N.; Xu, C.; Retter, R. W.; Bell, M.; Hilgenbrink, A.; Bakker, E. *Adv. Mater.* **2007**, *19*, 1059–1063.
(3) Feng, J.; Wang, B.; Gao, C.; Shen, J. *Adv. Mater.* **2004**, *16*, 1940–1944.
(4) Ma, Y.; Dong, W. F.; Hempenius, M. A.; Möhwald, H.; Vancso, G. J. *Nat. Mater.* **2006**, *5*, 724–729.
(5) Lvov, Y.; Antipov, A. A.; Mamedov, A.; Mo1hwald, H.; Sukhorukov, G. B. *Nano Lett.* **2001**, *1*, 125–128.
(6) Dong, W. F.; Ferri, J. K.; Adalsteinsson, T.; Schönhoff, M.; Sukhorukov, G. B.; Möhwald, H. *Chem. Mater.* **2005**, *17*, 2603–2611.
(7) Decher, G. *Science* **1997**, *277*, 1232–1237.
(8) Angelatos, A. S.; Johnston, A. P. R.; Wang, Y.; Caruso, F. *Langmuir* **2007**, *23*, 4554–4562.
(9) Shutava, T.; Prouty, M.; Kommireddy, D.; Lvov, Y. *Macromolecules* **2005**, *38*, 2850–2858.
(10) Jomaa, H. W.; Schlenoff, J. B. *Macromolecules* **2005**, *38*, 8473–8480.
(11) Lvov, Y. M.; Lu, Z.; Schenkman, J. B.; Zu, X.; Rusling, J. F. *J. Am. Chem. Soc.* **1998**, *120*, 4073–4080.
(12) Yoo, D.; Shiratori, S. S.; Rubner, M. F. *Macromolecules* **1998**, *31*, 4309–4318.
(13) Dubas, S. T.; Schlenoff, J. B. *Macromolecules* **2001**, *34*, 3736–3740.
(14) De Geest, B. G.; Déjugnat, C.; Verhoeven, E.; Sukhorukov, G. B.; Jonas, A. M.; Plain, J.; Demeester, J.; De Smedt, S. C. *J. Controlled Release* **2006**, *116*, 159–169.
(15) Ibarz, G.; Dähne, L.; Donath, E.; Möhwald, H. *Adv. Mater.* **2001**, *13*, 1324–1327.
(16) Ye, S.; Wang, C.; Liu, X.; Tong, Z.; Ren, B.; Zeng, F. *J. Controlled Release* **2006**, *112*, 79–87.
(17) Ai, H.; Jones, S. A.; de Villiers, M. M.; Lvov, Y. M. *J. Controlled Release* **2003**, *86*, 59–68.
(18) Breimer, D. D. *J. Controlled Release* **1999**, *62*, 3–6.
(19) Köhler, K.; Möhwald, H.; Sukhorukov, G. B. *J. Phys. Chem. B* **2006**, *110*, 24002–24010.
(20) Ichikawa, H.; Fukumori, Y. *J. Controlled Release* **2000**, *63*, 107–119.
(21) Kidchob, T.; Kimura, S.; Imanishi, Y. *J. Controlled Release* **1998**, *50*, 205–214.
(22) Yu, A.; Wang, Y.; Barlow, E.; Caruso, F. *Adv. Mater.* **2005**, *17*, 1737–1741.
(23) Shchukin, D. G.; Ustinovich, E. A.; Sukhorukov, G. B.; Möhwald, H.; Sviridov, D. V. *Adv. Mater.* **2005**, *17*, 468–472.
(24) Narita, T.; Yamamoto, T.; Suzuki, D.; Dobashi, T. *Langmuir* **2003**, *19*, 4051–4054.
(25) Akamatsu, K.; Yamaguchi, T. *Ind. Eng. Chem. Res.* **2007**, *46*, 124–130.
(26) Feng, Z.; Wang, Z.; Gao, C.; Shen, J. *Chem. Mater.* **2007**, *19*, 4648–4658.
(27) An, Z.; Möhwald, H.; Li, J. *Biomacromolecules* **2006**, *7*, 580–585.
(28) Tong, W.; Gao, C.; Möhwald, H. *Macromolecules* **2006**, *39*, 335–340.
(29) Angelatos, A. S.; Radt, B.; Caruso, F. *J. Phys. Chem. B* **2005**, *109*, 3071–3076.
(30) Yuan, X.; Fischer, K.; Schärtl, W. *Langmuir* **2005**, *21*, 9374–9380.

10.1021/la801138e CCC: $40.75
Published on Web 09/23/2008

Microcapsules can also be functionalized by magnetic nanoparticles for enhanced therapeutic performance or to impart recognition property with functional molecules to perform targeting delivery. Once arrived at the targeted site, a method to control the release of the active substances from the functionalized microcapsules with therapeutically effective dosage becomes important. Among the methods, drug release through the use of ultrasound and laser-light illumination has been reported.[32,33,35,36] For the ultrasonication method, morphological change of the capsule wall occurs due to the shear forces induced between the successive fluid layers, resulting in the disruption of the capsule shell. The principle of laser-light illumination is based on heating of metal nanoparticles, which alters the permeability of the capsule's shells through absorption of the laser-induced heat from the gold nanoparticles within shells and finally released encapsulated materials. These laser-sensitive microcapsules can be applied, after cellular uptake, for transdermal drug delivery.[37] Recently, Wu et al. reported the remotely triggered liposome release by near-infrared light absorption via hollow gold nanoparticles. With femtosecond pulses of NIR light stimulus, those liposomes can release drug within seconds.[38]

Herein, a novel magnetic-sensitive microcapsule is designed via the use of high-frequency magnetic field (HFMF) to trigger the release of drug from the microcapsule. The microcapsule is composed of multilayer shell (or wall) structure with magnetic nanoparticles, i.e., hereinafter termed "nanomagnets", embedded into the capsule walls in order to achieve a controllable release operation under HFMF. Numerous studies have used magnetic nanoparticles for a number of medical and biological applications, such as drug/gene delivery,[39] bioseparation,[40] magnetic resonance imaging,[41] and hyperthermia therapy.[42] Li et al. reported a pH-responsive drug release of magnetic microcapsules.[43] Recently, polyelectrolyte-based microcapsules embedded with Co/Au can be activated by using an external magnetic field of 100−300 Hz to modulate its permeability.[44] Under such alternative magnetic fields, the capsule's permeability was increased, and it then absorbed active macromolecules from the environment. To our best knowledge, using a magnetic field to manipulate the degradation behavior of microcapsules for controlled drug release has rarely been reported. The principal concept of the investigation is schematically shown in Figure 1, where the nanomagnet-containing polyelectrolyte microcapsules were synthesized in this work and the effect of HFMF on the evolution of its microstructure was explored. Accordingly, a high-frequency magnetic field of 50−100 kHz accelerates the rotation and motion of the embedded iron oxide nanoparticles, i.e., nanomagnets, with moderate heat generation, which subsequently causes a conformational change of the polyelectrolyte molecule chains, resulting in rupturing the capsules, which is followed by a rapid release of the entrapped substances. The release kinetics of the drug will therefore be governed by the degradation profile of the capsule walls. This study is then aimed to provide proof-of-concept on designing the "remote-rupturing microcapsules" for controlled release of active substance through external magnetic stimuli.

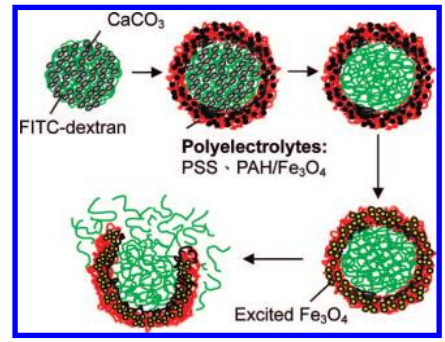

Figure 1. Schematic representation of the encapsulation and release of substances in polyelectrolyte capsules. Calcium carbonate microspheres with fluorescein isothiocyanate−dextran as the cores are coated with polyelectrolytes and nanoparticles using a layer-by-layer technique. After dissolution of the calcium carbonate, the hollow capsules are obtained. After a magnetic field treatment, the capsules should rupture and release the encapsulated substances.

Experimental Section

Materials. Calcium chloride dihydrate ($CaCl_2 \cdot 2H_2O$, MW = 147.01 g/mol, ≥99%, Sigma), sodium carbonate (Na_2CO_3, MW = 105.99 g/mol, ≥99%, Sigma), sodium chloride (NaCl, MW = 58.44 g/mol, ≥99.5%, Fluka), poly(sodium 4-styrene sulfonate) (PSS, MW = 70 kDa, Sigma), and poly(allylamine hydrochloride) (PAH, MW = 70 kDa, Aldrich) were used for LbL assembly. Rhodamine B isothiocyanate (RITC, MW = 536.08 g/mol, Fluka) and fluorescein isothiocyanate−dextran (FITC−dextran, MW = 20 kDa, Sigma) were used for labeling, which helps capsule visualization under fluorescence microscope and confocal laser scanning microscopy (CLSM). RITC-labeled PAH was prepared as reported in the literature.[45] Doxorubicin hydrochloride (Doxo, MW = 579.98 g/mol, ≥98%, Fluka) was used as the model drug. Ethylenediaminetetraacetic acid (EDTA, MW = 292.24 g/mol, 99.995%, Aldrich) was used to remove the $CaCO_3$. Ferrous chloride tetrahydrate ($FeCl_2$, >99.0%(RT), Fluka) and iron(III) chloride hexahydrate ($FeCl_3$, Riedel-deHaen) were used to synthesized the iron oxide nanoparticles. Citric acid (MW = 192.12 g/mol, ≥99.5%, Fluka) was used to modify iron oxide nanoparticles. All chemicals were purchased and used without further treatments.

Preparation of Iron Oxide Nanoparticles. The iron oxide nanoparticles were prepared in a water solution without any stabilizer as outlined by Mikhaylova et al.[46] Typically, 0.2 M $FeCl_3 \cdot 6H_2O$ and 0.1 M $FeCl_2 \cdot 4H_2O$ with a $FeCl_2/FeCl_3$ molar ratio of 2:1 were dissolved into 50 mL of water with vigorous stirring at room temperature. Ammonium water (10 mL of 33% NH_4OH) was added to cause precipitation, wherein the Fe_3O_4 nanoparticles were immediately formed in the solution. The precipitated powders were collected and removed from the solution and then washed by 200 mL of deionized water three times. The magnetic nanoparticles were

(31) Shchukin, D. G.; Köhler, K.; Möhwald, H. *J. Am. Chem. Soc.* **2006**, *128*, 4560–4561.
(32) Shchukin, D. G.; Gorin, D. A.; Möhwald, H. *Langmuir* **2006**, *22*, 7400–7404.
(33) De Geest, B. G.; Skirtach, A. G.; Mamedov, A. A.; Antipov, A. A.; Kotov, N. A.; De Smedt, S. C.; Sukhorukov, G. B. *Small* **2007**, *3*, 804–809.
(34) De Geest, B. G.; Jonas, A. M.; Demeester, J.; De Smedt, S. C. *Langmuir* **2006**, *22*, 5070–5074.
(35) Skirtach, A. G.; Dejugnat, C.; Braun, D.; Susha, A. S.; Rogach, A. L.; Parak, W. J.; Möhwald, H.; Sukhorukov, G. B. *Nano Lett.* **2005**, *5*, 1371–1377.
(36) Radt, B.; Smith, T. A.; Caruso, F. *Adv. Mater.* **2004**, *16*, 2184–2189.
(37) Skirtach, A. G.; Javier, A. M.; Kreft, O.; Köhler, K.; Alberola, A. P.; Möhwald, H.; Parak, W. J.; Sukhorukov, G. B. *Angew. Chem., Int. Ed.* **2006**, *45*, 4612–4617.
(38) Wu, G.; Mikhailovsky, A.; Khant, H. A.; Fu, C.; Chiu, W.; Zasadzinski, J. A. *J. Am. Chem. Soc.* **2008**, *130*, 8175–8177.
(39) Nasongkla, N.; Bey, E.; Ren, J.; Ai, H.; Khemtong, C.; Guthi, J. S.; Chin, S. F.; Sherry, A. D.; Boothman, D. A.; Gao, J. *Nano Lett.* **2005**, *6*, 2427–2430.
(40) Doyle, P. S.; Bibette, J.; Bancaud, A.; Viovy, J. L. *Science* **2002**, *295*, 2237.
(41) Huh, Y. M.; Jun, Y. W.; Song, H. T.; Kim, S.; Choi, J. S.; Lee, J. H.; Yoon, Y.; Kim, K. S.; Shin, J. S.; Suh, J. S.; Cheon, J. *J. Am. Chem. Soc.* **2005**, *127*, 12387–12391.
(42) Jordan, A.; Scholz, R.; Wust, P.; Schirra, H.; Schiestel, T.; Schmidt, H.; Felix, R. *J. Magn. Magn. Mater.* **1999**, *194*, 185–196.
(43) Li, L. L.; Chen, D.; Ding, M. H.; Tang, F. Q.; Meng, X. W.; Ren, J.; Zhang, L. *Acta Phys.-Chim. Sin.* **2007**, *23*, 1969.
(44) Lu, Z.; Prouty, M. D.; Guo, Z.; Golub, V. O.; Kumar, C. S. S. R.; Lvov, Y. M. *Langmuir* **2005**, *21*, 2042–2050.
(45) Zhu, H.; Srivastava, R.; McShane, M. J. *Biomacromolecules* **2005**, *6*, 2221–2228.
(46) Mikhaylova, M.; Kim, D. K.; Bobrysheva, N.; Osmolowsky, M.; Semenov, V.; Tsakalakos, T.; Muhammed, M. *Langmuir* **2004**, *20*, 2472–2477.

separated by centrifugation, and the average particle size was estimated to be around 6 nm on the basis of the X-ray diffraction (XRD, M18XHF, Mac Science) measurements. On the other hand, 2 wt % citric acid was used to modify the iron oxide nanoparticles.[47] With the citric acid treatment for 1 day, the iron oxide particles possessed negative charges on their surfaces. The excess acid was removed by deionized water three times.

Polyelectrolyte Microcapsules. The cores of the microcapsules were fabricated by calcium carbonate microspheres. In brief, $CaCl_2$ and Na_2CO_3 solutions (0.33 M) were mixed under vigorous stirring for 60 s, which led to the precipitation of $CaCO_3$ microspheres. And then, the microspheres were washed with deionized water four times to remove the unreacted species and separated by the centrifugation. Finally, the particles were washed with acetone and dried in ambient condition. FITC−dextran was incorporated in the $CaCO_3$ microspheres through a coprecipitation process: 5 mg of FITC−dextran was dissolved in 3.5 mL of $CaCl_2$ solution in the beginning, and after mixing with the Na_2CO_3 solution, the FITC−dextran is incorporated in the $CaCO_3$ microspheres.

Microcapsules were prepared via a two-step procedure. In the first step, 20 mg of FITC−dextran containing $CaCO_3$ microspheres was dispersed in a 0.5 M NaCl solution with 1 mg/mL PSS (i.e., polyanion) or Fe_3O_4 nanoparticles (citric acid modified, 1 mg mL^{-1}). The dispersed solution was continuously shaken for 10 min. The excess polyanion or Fe_3O_4 nanoparticles were removed by centrifugation/washing with deionized water. Then, 1 mL of 0.5 M NaCl solution containing RITC-labeled PAH (2 mg mL^{-1}) was added and continuously shaken for 10 min, followed again by the centrifugation and washing steps. The deposition process of oppositely charged polyelectrolyte was repeated four times, and four bilayers are deposited on the surface of the $CaCO_3$ microspheres. In the second step after the shell structure was formed, 0.2 M EDTA solution was used to remove the $CaCO_3$ core, where the core−shell microspheres were dispersed in the 10 mL EDTA solution (pH 5) and shaken for 4 h, followed by centrifugation and redispersion in fresh EDTA solution. This core-removing process was repeated three times to ensure that the $CaCO_3$ cores were completely removed. Finally, the hollow microcapsules filled with FITC−dextran can be obtained in the water.

Microcapsule Characterization. The morphologies of microcapsules were examined using field emission scanning electron microscopy (FE-SEM, JEOL-6500) and transmission electron microscopy (TEM, JEM-2100). For SEM analysis, the capsules were dried on 0.5 × 0.5 cm silicon wafers. After drying, the microcapsules were coated with an ultrathin metal layer through platinum sputtering to enhance the image quality taken in the experiments. PL microscopy and CLSM were used to investigate the morphology and structure changes of the microcapsules embedded with iron oxide nanoparticles before and after applying a high-frequency magnetic field (HFMF). The experiments were performed in six-well plates by dispersing the microcapsules in phosphate-buffered saline (pH 7.4). The magnetization of the magnetic microcapsules was measured by a superconducting quantum interference device (SQUID, MPMS-XL7) at 298 K and ±8000 G applied magnetic field. Before SQUID analysis, the iron oxide nanoparticles and microcapsules were dried in a vacuum oven for 60 °C for 2 days. Photoluminescence (PL) spectroscopy (PL, fluorescence spectrophotometer F-4500, Hitachi) was used to characterize the release profile of the dye molecule by measuring the change in the intensity of the fluorescence dye before and after a high-frequency magnetic field (HFMF) of 50 kHz was applied to microcapsules with a concentration of 1 wt % dispersed in the water solution. HFMF was produced by power supply, functional generator, amplifier, and cooling water. The strength of the magnetic field depended on the coils. In this study, the coil is eight loops, the frequency is 50 kHz, and the strength of magnetic field (H) is 2.5 kA/m. The temperature of HFMF generator was controlled by cycling cooling water at 25 °C.

Drug Loading and Release. In this investigation, doxorubin hydrochloride was used as a model drug to estimate the drug release behaviors of the microcapsules. The microcapsules were washed with phosphate-buffered saline (pH 7.4), following by washing with deionized water. Doxo (0.2 wt %) was dissolved in the pH 5 buffer solution in advance. Doxo was loaded in microcapsules by exposing them to the Doxo solution for 12 h, followed by washing with water.[48] The doxorubicin can diffuse into the capsules in the pH 5 buffer solution. The results have been studied by other groups.[27,28] This is because of the change of the polyelectrolyte charges upon pH variation, loosening the polyelectrolyte networks and inducing the pore formation. Therefore, a high concentration of drug molecules can penetrate into capsules. The quantitative estimation of the Doxo loading was obtained by a UV−vis spectrophotometer. The drug release behavior from the microcapsules was measured in 20 mL of phosphate-buffered saline per sponge cube (pH 7.4). To measure the concentration of drug release, 1.5 mL of PBS medium with the dispersed microcapsules was taken out and separated by centrifugation at 4000 rpm. The clear solution without microcapsules was used to estimate the concentration of drug release. UV−visible spectroscopy (Agilent, 8453 UV−visible spectrophotometer) was used for characterization of the absorption peak at 480 nm (I_{max} of free Doxo). The microcapsules were absent and did not affect the measurements.

Cell Culture. A549 (lung carcinoma) cells were maintained in DMEM (Dulbecco's modified Eagle's medium) containing 10% fetal bovine serum, 100 units/mL penicillin, and 100 μg/mL streptomycin. Cells were cultured with complete medium at 37 °C in a humidified atmosphere of 5% CO_2 in air. For all of the experiments, cells were harvested from subconfluent cultures by use of trypsin and were resuspended in fresh complete medium before plating. A comparison of in vitro cytotoxicity of microcapsules with different concentrations and times was performed on A549 cells with an in vitro proliferation method using MTT [3-(4,5-dimethyldiazol-2-yl)-2,5 diphenyl tetrazolium bromide].[49] Briefly, 1×10^4 cells were plated in 96-well plates to allow the cells to attach and then exposed to the serial concentrations of microcapsules at 37 °C. At the end of the incubation, 20 μg of MTT solution was added and incubated for another 4 h. Then, the medium was replaced with 200 μg of DMSO and the absorbance was monitored using a Sunrise absorbance microplate reader at dual wavelengths of 570 and 650 nm.

Results and Discussion

Preparation of Microcapsules. Two types of microcapsules were prepared, one is solely composed of PAH/PSS polyelectrolytes, as shown in Figure 2a,b, and the other is a hybrid structure consisting of iron oxide (Fe_3O_4) nanoparticles and PAH polyelectrolyte (Figure 2c,d). Fe_3O_4 nanoparticles, having a diameter ranging from 5 to 8 nm (see Supporting Information, Figure S2), used in this system were prepared according to the method reported by Mikhaylova et al.[46] The $(PSS/PAH)_4$ microcapsules displayed a smoother surface morphology compared to the $(Fe_3O_4/PAH)_4$ microcapsules, which is due to the presence of the iron oxide nanoparticles that distributed throughout the thin polyelectrolyte layer, and the nanoparticles provide rigid structure and procures a rather rough surface after drying. The incorporation of iron oxide nanoparticles also caused the shells of the microcapsules to be mechanically stronger, resulting in better structural integrity, as evidenced in Figure 2c,d, than the one without the nanoparticles. The resulting Fe_3O_4 nanoparticles have a size of 5 nm on average dispersed in the polyelectrolyte shell (Figure 2e), where no defects such as crevices were visually detected at the interfacial regions. Photoluminescence (PL) microscopy (Figure 2f) also revealed that the $(Fe_3O_4/PAH)_4$ microcapsules, with an average diameter of 4 μm, were well-dispersed in the solution. These results demonstrated that the $(Fe_3O_4/PAH)_4$ microcapsules were successfully prepared in this

(47) Grigoriev, D.; Gorin, D.; Sukhorukov, G. B.; Yashchenok, A.; Maltseva, E.; Möhwald, H. *Langmuir* **2007**, *23*, 12388–12396.
(48) Khopade, A. J.; Caruso, F. *Biomacromolecules* **2002**, *3*, 1154–1162.
(49) Mosmann, T. *J. Immunol. Methods* **1983**, *65*, 55–63.

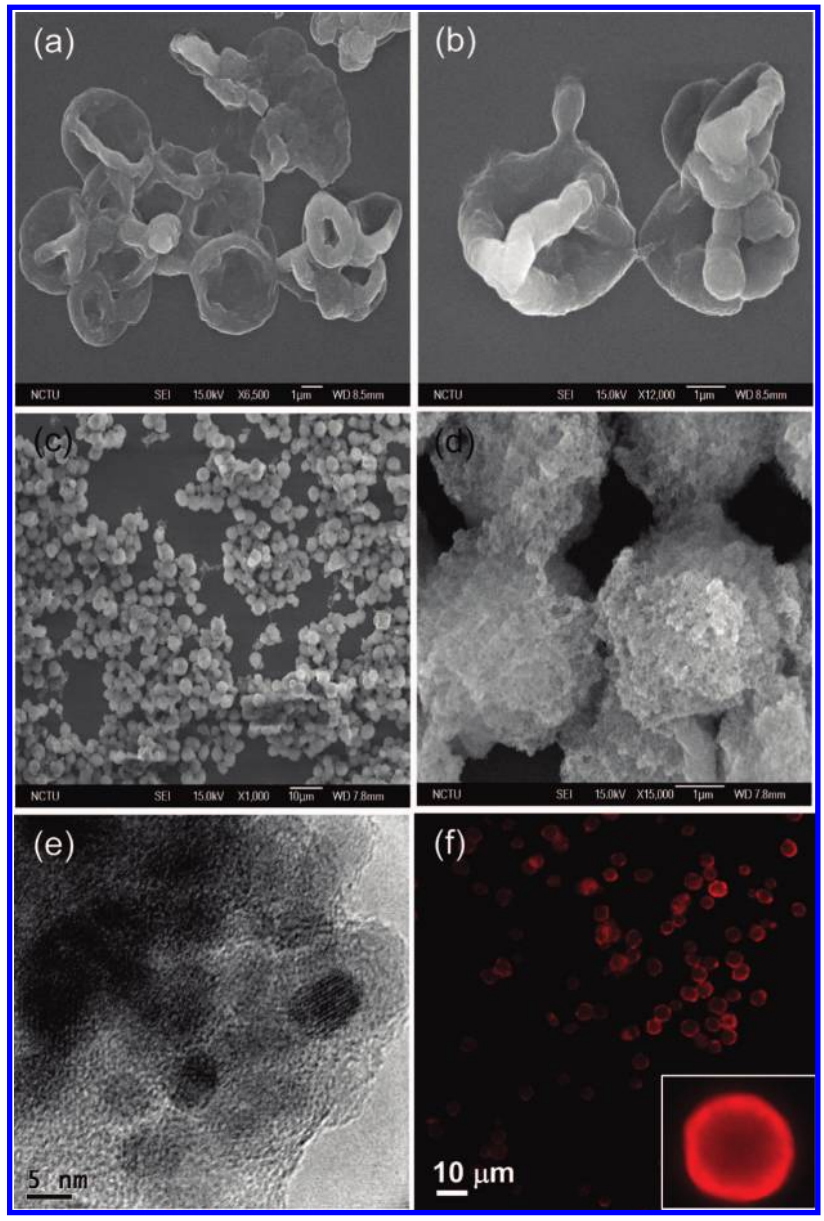

Figure 2. SEM images of (a, b) $(PSS/PAH)_4$ capsules and (c, d) $(Fe_3O_4/PAH)_4$ capsules. (e) TEM image of $(Fe_3O_4/PAH)_4$ capsules. (f) PL microscopy image of $(Fe_3O_4/PAH)_4$ capsules.

study. The inset of Figure 2f shows a higher magnification image to demonstrate the capsule's structure.

Magnetic Property of the Microcapsules. The magnetic property of the $(Fe_3O_4/PAH)_4$ microcapsules was studied by a superconducting quantum interference device (SQUID, MPMS-XL7) at ambient temperature with the magnetic field sweeping from −8000 to +8000 G. Figure 3 shows the correlation of the magnetization with magnetic field for iron oxide nanoparticles and the $(Fe_3O_4/PAH)_4$ microcapsules, where both curves show similar shape with negligible hysteresis. However, the microcapsule, i.e., 17 emu/g (as high as 35 wt % of Fe_3O_4 in the shell structure via TGA), showed much less saturation magnetization (M_s) than the nanoparticles, i.e., 53 emu/g, which is due to the presence of polyelectrolytes that dilute the concentration of Fe_3O_4 nanoparticles. The remanences of $(Fe_3O_4/PAH)_4$ capsules and iron oxide nanoparticles are 0.19 and 0.83 emu/g, respectively. The coercive forces of $(Fe_3O_4/PAH)_4$ capsules and iron oxide nanoparticles are 29.4 and 23.6 Oe, respectively (see Supporting Information).

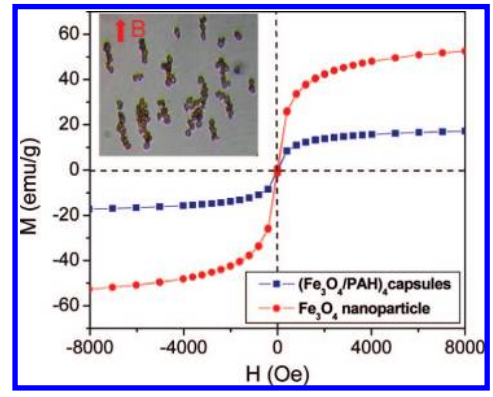

Figure 3. Field-dependent magnetization curve of $(Fe_3O_4/PAH)_4$ capsules and iron oxide nanoparticles. Inset: the $(Fe_3O_4/PAH)_4$ capsules aligned with the magnetic field.

FITC−Dextran Release Behaviors with HFMF Treatment. In order to monitor the release behavior of the $(Fe_3O_4/PAH)_4$ microcapsules under HFMF stimulus, FITC−dextran molecules

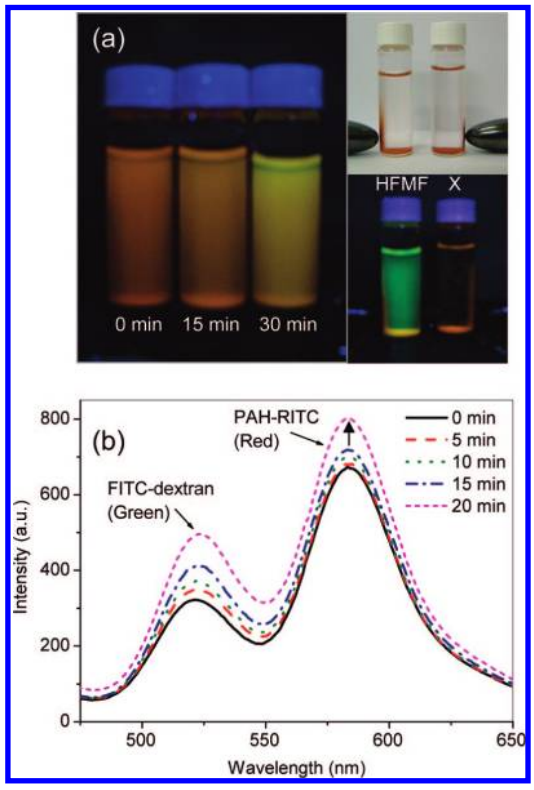

Figure 4. (a) Photographs of the bottles with fluorescence-loaded $(Fe_3O_4/PAH)_4$ capsules dispersed in water solution. Before HFMF exposure, fluorescence-loaded $(Fe_3O_4/PAH)_4$ capsules displayed deep-orange fluorescence under the UV light (left, 0 min). After HFMF exposure, green fluorescence was released from these capsules, and then, the color of the solution changed to orange and yellow under UV-light (15 and 30 min). Right panel: after the $(Fe_3O_4/PAH)_4$ microcapsules were subjected to 30-min (labeled as "HFMF") and 0-min (labeled as "X") HFMF stimulus, a magnet was used to aggregate the microcapsules to side wall of the glass bottle; afterward, a green color, the primary color of the FITC−dextran substance, appeared in the bottle under UV illumination. (b) Emission spectra of fluorescence-loaded $(Fe_3O_4/PAH)_4$ capsules upon applying HFMF from 0 to 20 min.

with green fluorescence dyes were incorporated in the microcapsules, and RITC (red fluorescence dye) was used to label the PAH on the shell structure. Through RITC molecules bound on the shells, the geometric changes of the shell structure can be visually monitored under PL illumination. Furthermore, the color change of the solution due to molecular (FITC−dextran) release and the variation of the microcapsule's structure can be characterized in a real-time approach while the $(Fe_3O_4/PAH)_4$ microcapsules were subjecting to the HFMF. Figure 4a shows the $(Fe_3O_4/PAH)_4$ microcapsules suspended in the PBS solution with different durations of HFMF treatment. The dye was excited under UV illumination, and the color of the solution then changed with the duration of the magnetic stimulus. The solution, prior to the stimulus, showed deep-orange appearance, which is attributed to the color of the RITC−PAH phase, indicating that the core substances, i.e., FITC−dextran, were stably enclosed within the $(Fe_3O_4/PAH)_4$ shell without a sign of leakage or release. The change in solution color, from orange to yellow with increasing time of the stimulus indicates the FITC−dextran being released through the $(Fe_3O_4/PAH)_4$ shell. In Figure 4a (right), after the $(Fe_3O_4/PAH)_4$ microcapsules were subjected to 30-min (labeled as "HFMF" in right panel of Figure 4a) and 0-min (labeled as "X" in the right panel of Figure 4a) HFMF stimulus, a magnet was used to aggregate the microcapsules to the side wall of the glass bottle; afterward, a green color, the primary color of the FITC−dextran substance, appeared in the bottle under UV illumination (bottom picture), indicating that the FITC−dextran was effectively released from the core phase to the environment under magnetic stimulus. In contrast, for the $(Fe_3O_4/PAH)_4$ microcapsules with 0-min stimulus, no sign of FITC−dextran was visually detected under UV illumination, which indicated that the FITC−dextran molecules were encapsulated in the microcapsules without crossing the shell, even after a long-term exposure (6 h) in the solution.

The PL spectroscopy is shown in Figure 4b, where two independent characteristic peaks at 523 nm (FITC−dextran) and 583 nm (RITC−PAH) were detected. While subjecting to the stimulus, the concentration of the FITC−dextran increased, as depicted by a corresponding increase in the spectral intensity of green fluorescence, with the increased time of stimulus. In the meantime, the spectral intensity of red fluorescence (RITC−PAH) was also increased, suggesting that the RITC−PAH shell is dissociated structurally under the magnetic stimulus. It seems that in the first 5 min of stimulus, the FITC−dextran molecules started to release from the microcapsules. Up to 10 min, the intensity of the red fluorescence dye increased, suggesting that the shell structure underwent dissociation. The intensity of the red fluorescence dye became more pronounced after then, till 20 min of the stimulus, indicating that the microcapsule shells structurally dissociated to a considerable extent. The FITC−dextran released out from capsules, indicating that FITC−dextran was not shielded by the capsule shells, so the intensity of the green fluorescence light increased. The intensity of the red fluorescence light was also increased obviously, which may due to the $(Fe_3O_4/PAH)_4$ membranes being destroyed or deformed under HFMF. The membranes' morphologies and structures should be affected by the HFMF and, therefore, change the absorbance of the red fluorescence dye. This finding suggests that the presence of the nanomagnets, within the polyelectrolyte shell, is able to dissociate the shells' structure either physically or chemically or a mix of both, which is subject to confirmation in the forthcoming analysis. However, it is believed from this study that the embedded nanomagnets are capable of manipulating the microstructure of the polyelectrolyte shell, and this permits the accessibility of the active substances enclosed in the core phase to release across the shell in a controllable manner, from a relative slow profile to a burstlike profile, depending upon the magnetically induced microstructural or nanostructural evolution of the shell.

Doxorubicin Release Behavior. While the magnetically induced dye release and the corresponding spectroscopic observation of microstructural evolution were experimentally confirmed, a DOX-loaded microcapsule sample was prepared for release profile investigation. Figure 5 shows a significant increase in the amount of DOX released under a magnetic stimulus (black squares). In comparison to the DOX-loaded $(PSS/PAH)_4$ and $(Fe_3O_4/PAH)_4$ microcapsules in the absence of HFMF, the DOX release rates were much slower compared to the microcapsules under magnetic stimulus. The $(PSS/PAH)_4$ microcapsules possessed a smooth and dense shell structure, which is accountable for a relatively slow diffusion of DOX across the shell; therefore, after 40 min of release, the cumulative released amount of the DOX was estimated to be ~3% from the $(PSS/PAH)_4$ microcapsules. For the $(Fe_3O_4/PAH)_4$ microcapsules, the cumulative released amount is about 9%, which is believed to result from a rough shell structure. Comparatively, in the presence of the magnetic stimulus, the cumulative released amount is effectively increased to about 67% over a 30-min operation, suggesting that the microstructure of the shell of the $(Fe_3O_4/PAH)_4$ microcapsules is physically deteriorated upon stimulus, as evidenced above, resulting in a much faster DOX release.

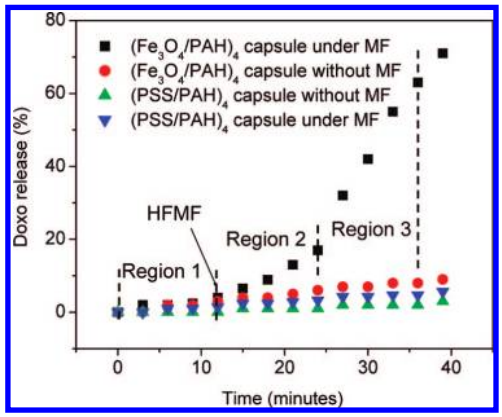

Figure 5. Drug release profiles of $(Fe_3O_4/PAH)_4$ capsules triggered by a HFMF, from 12 to 39 min (black squares). The control groups of $(PSS/PAH)_4$ capsules without magnetic iron incorporation and $(Fe_3O_4/PAH)_4$ capsules without HFMF treatment are also shown (green triangle and red circles).

This finding strongly indicates that the applied HFMF accelerated considerably the drug release from the $(Fe_3O_4/PAH)_4$ microcapsules by as large as about 7 times compared to that without the stimulus. This considerable increase in the release profile is unlikely to be diffusion-dominated; in other words, the DOX release through the shell barrier is enhanced, where the barrier nature of the shell structure is diminished to a considerable extent. If comparing to the microstructural evolution monitored using dye molecules as aforementioned, this enhancement in the release profile can be a direct indication of the structural dissociation of the shell under magnetic force.

After a closer look at the drug release profiles of the $(Fe_3O_4/PAH)_4$ microcapsules under HFMF, the graph can be divided into three regions of release pattern, as illustrated in Figure 5. In region 1, where the pattern corresponds to the microcapsule without the application of the magnetic field, the cumulative release of DOX is 4%. In regions 2 and 3, upon being subjected to the field, the DOX release reaches to a level of 13% and up to 45%, respectively, under the same duration of stimulus. These two regions of release kinetics, if simply approximated as a linear release pattern over a short period of time, then estimated that the drug release rate over the region 3 is nearly 3.5 times faster than that of region 2, suggesting that a transition of the release kinetics takes place while the magnetically induced energy is cumulatively exerted upon the microcapsules. This transition in release profile is believed to be essential as a result of the microstructural transition of the shell structure of the microcapsules, facilitating DOX release. A real-time, HFMF-responsive drug delivery can be achieved, and it is believed that the rapid responsiveness of the $(Fe_3O_4/PAH)_4$ microcapsules with respect to the HFMF stimulus is able to offer greater potential for an in-time drug release device for medical applications.

Microstructural Evolution under Magnetic Stimulus. Figure 6shows that the surface morphology of the as-synthesized microcapsules in the absence of the magnetic field showed no visually observable cracks or crevices. However, after 10-min stimulus, a certain amount of nanocavities of 50−100 nm in size appeared on the surface of the microcapsules (Figure 6a); however, the shape of the microcapsules was remained the same as original dimension. These nanocavities are unlikely to be resulting from dissolution of the polyelectrolyte in the aqueous solution but

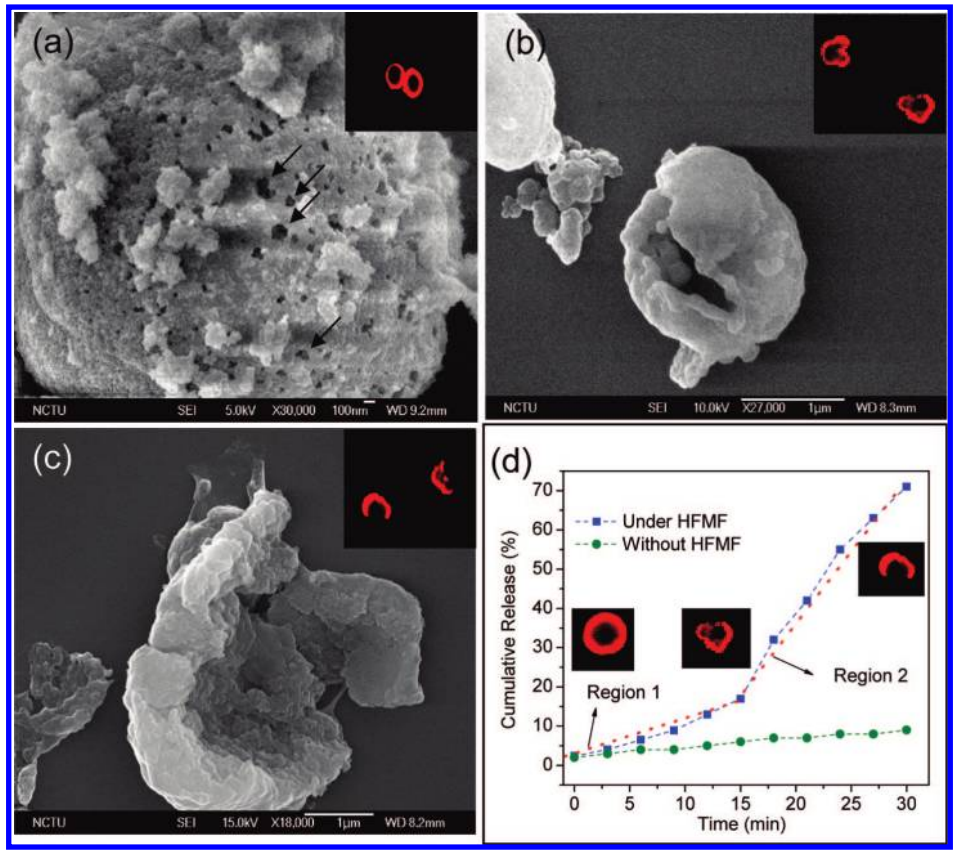

Figure 6. SEM and CLSM images of $(Fe_3O_4/PAH)_4$ capsules after HFMF treatment for (a) 10 min, (b) 15 min, and (c) 30 min. After 10-min stimulus, a certain amount of nanocavities 50−100 nm in size appeared on the surface of the microcapsules. Upon further increasing the HFMF stimulus to 30 min, the microcapsules were ruptured to a large extent. (d) The drug release behavior and morphologies of $(Fe_3O_4/PAH)_4$ capsules under continue HFMF.

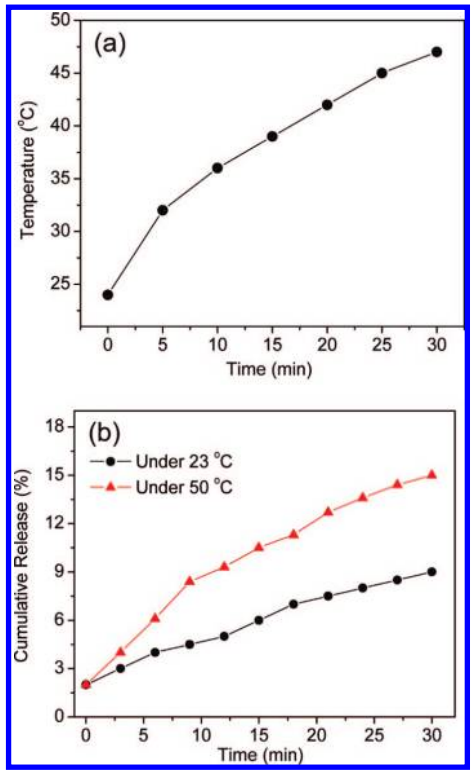

Figure 7. (a) Temperature increase curve of $(Fe_3O_4/PAH)_4$ capsules when applying the HFMF. (b) The drug release behaviors of $(Fe_3O_4/PAH)_4$ capsules under HFMF, upon heating to 50 °C and room tempearature for 30 min.

may be resulting from thermally induced dissociation, although there is no direct evidence for this at the present, since the high-frequency magnetic field is able to induce heat generation at a faster rate than low-energy field within the shell, and some "hot-spots" can develop within the shell region. Such hot spots are believed to effectively induce a dissociation of the shell structure.

After 15 min, numerous cracks appeared on the microcapsule surface, as illustrated in Figure 6b. The CLSM images also illustrated that the geometry of the microcapsules can no longer keep a spherical shape as first prepared; instead, the microcapsules were seriously deformed, and some regions formed cracks, as illustrated in the CLSM image. After 30 min of stimulus, the microcapsules were ruptured to a large extent, as shown in Figure 6c. The rupture of the microcapsules caused a dramatic increase in the drug release behavior (Figure 7d). Corresponding to the microstructural evolution of the microcapsules under magnetic stimulus, the DOX release profile can be separated into two regions. In region 1, the capsules still maintained their structural integrity but only produced some nanopores on the surface, causing a slow and steady releasing. This explains why the surface nanopores have little or no contribution to alter drug release profile. Since those nanopores are located on the shell of the microcapsules, this suggests that the pores are virtually generated due to the action of the nanomagnets upon magnetic stimulus. However, after 15 min of HFMF treatment, a burst release can be followed in region 2, where the DOX released rapidly because of the magnetically induced rupture of the microcapsules. The release rate of region 2 is higher by about 7 times than that of region 1, corresponding to a significant change in the microstructure of the shell.

The rationale behind the rupture of the microcapsules due to the presence of the nanomagnets is believed to be a result of the energy absorption by the nanomagnets induced by the incident magnetic field, and we believed it may result from a continuous evolution of the nanocavity on the surface, although the nature of nanocavity growth is not fully understood at present, it appears that until a percolation of the cavities has been achieved, no crack of consequence can develop. Growth of the crack due to both nanocavity development and, in the meantime, the vibration and vigorous motion of the nanomagnets within the thin shell under the high-frequency magnetic field stimulus will then result in a final mechanical rupture of the shell. It was reported that the heating power, governed by the mechanism of magnetic energy dissipation for single-domain particles (Brown and Néel relaxations), is highly sensitive to the crystal size and the material.[50] In such a way, the degree and speed of deformation and/or rupture of the polyelectrolyte shell with the nanomagnets inside the shell structure should depend on the interaction among the nanomagnets themselves and their distribution in the shell.

Experimental observations suggest that such a HFMF-induced microstructural evolution involves the following three stages: (i) heating of the microcapsule shell locally to cause a certain degree of relaxation of polyelectrolytes, which further causes (ii) cavity or pore formation, followed by (iii) rupture of the microcapsule shell. The latter two have been experimentally verified. To further verify the heating effect, i.e., causing a temperature rise, investigation was carried out to measure the temperature rise due to magnetic stimulus on the $(Fe_3O_4/PAH)_4$ microcapsule-containing solution. One weight percent of the $(Fe_3O_4/PAH)_4$ microcapsules dispersed in the water solution were applied with HFMF. The strength of the magnetic field depended on the coils. In this study, the coil is eight loops, the frequency is 50 kHz, and the strength of the magnetic field (H) is 2.5 kA/m. For 30 min of stimulus, a 23 °C increment (from 23 to 46 °C) of the solution was observed, as illustrated in Figure 7a. The sample with identical composition of the $(Fe_3O_4/PAH)_4$ microcapsules was heated to 50 °C for 30 min in a comparative study, and the drug release behavior was monitored concurrently and compared with the $(Fe_3O_4/PAH)_4$ microcapsules with and without HFMF given in Figure 5b. Below 50 °C, the $(Fe_3O_4/PAH)_4$ microcapsules released about 15% of DOX, which was higher by 9% than those microcapsules released at room temperature. The result suggests that the $(Fe_3O_4/PAH)_4$ microcapsules become structurally unstable with increasing temperature, where a relaxation of the polyelectrolyte may be induced, resulting in an increase of DOX diffusion. Therefore, while applying the HFMF to the microcapsules, the heat induced by HFMF played an important role to accelerate the drug release, because the relaxations of polyelectrolyte on the capsules or increasing the kinetics of the drug molecules caused the drug release from the microcapsules.

An alternative mechanism is that the microcapsules in the magnetic field would be subjected to stretching along the direction of the field due to the magnetostatic energy,

$$E_{ms} = 1/2(N_{||} - N_{\perp})M^2V \quad (1)$$

where $N_{||}$ and $N_{\perp}$ are demagnetizing factors in the directions parallel and perpendicular to the magnetic field. E_{ms} is the energy of magnetic interaction of the magnetic moment M of the nanoparticles with magnetic field H. V is the volume of magnetic nanoparticles. Magnetostatic interactions induced by the magnetic field will lead to the appearance of a large demagnetizing field inside the capsule shells. Besides, the interaction between magnetic particles has been demonstrated to occur under an external magnetic field.[51] For two identical particles with magnetic

(50) Fortin, J. P.; Wilhelm, C.; Servais, J.; Ménager, C.; Bacri, J. C.; Gazeau, F. *J. Am. Chem. Soc.* **2007**, *129*, 2628–2635.

(51) Dai, J.; Wang, J. J.; Sangregorio, C.; Fang, J.; Carpenter, E.; Tang, J. *J. App. Phys.* **2000**, *87*, 7397–7399.

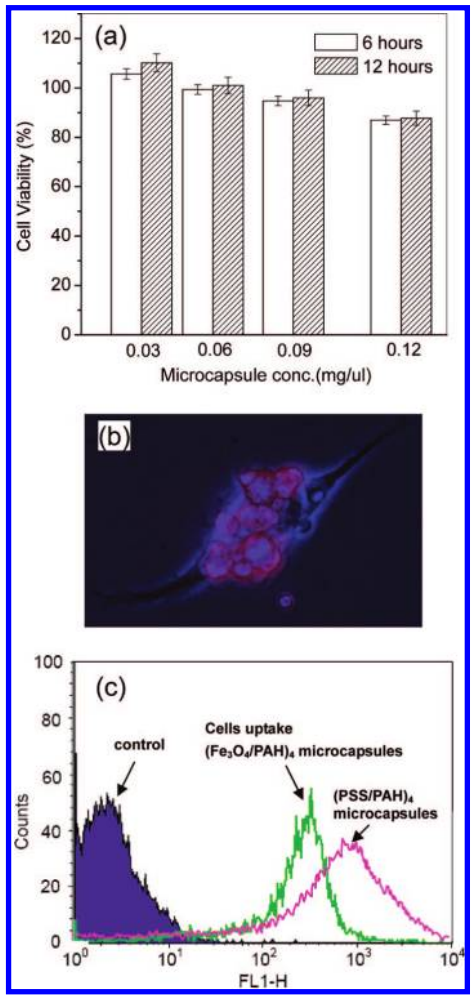

Figure 8. (a) Cell viability of A549 cells after 6 and 12 h of incubation with increasing amounts of $(Fe_3O_4/PAH)_4$ capsules. Cell viability was measured using an MTT assay. (b) Confocal microscopic images of A549 cells after contact with $(Fe_3O_4/PAH)_4$ capsules (0.05 mg/mL) for 6 h. (c) Fluorescence intensity of A549 cells after contact with $(Fe_3O_4/PAH)_4$ capsules (0.3 mg/mL).

moment M, interaction energy can be given as follows:

$$E_i \propto \frac{M^2}{r^3}(3 \cos \psi_1 \cos \psi_2 - \cos \alpha) \qquad (2)$$

where r is the distance between two particles, Ψ_1 and Ψ_2 are the angles between r and two moments, respectively, and α is the angle between the two moments. From eq 2, it is clear that the distance (r) between the magnetic nanoparticles is also strongly related to the intensity of interaction energy. Through this interaction, the magnetic particles embedded in the shell structure will tend to align along the direction of the magnetic field, resulting in establishing stresses inside the microcapsule walls. Such stresses may act as an important factor triggering and/or accelerating the formation of the nanocavities and also may play some role in pore size enlargement on the microcapsule walls and, most likely, also participating with the later-stage rupture of the walls. In consequence, by combining both the heating effect and the magnetically induced stress development within the shell structure, the permeability of magnetic capsules can be enhanced, and in the meantime, deformation and eventually rupture of the microcapsules take place at different stages of magnetic stimulus; however, either one of the stages is manipulated in a controllable manner, and this corresponds to different drug release profiles.

Cell Uptake. Cellular uptake of the polyelectrolyte capsules has been recently reported.[52,53] Such microcapsules can be attractive for drug delivery with an intracellular target like nucleic acid and various proteins. The results of the MTT assay, as a measure of metabolic competence of the cell with the $(Fe_3O_4/PAH)_4$ microcapsules with different concentrations, are shown in Figure 8a. The difference in the cytotoxicity at 6 and 12 h of incubation is negligibly small. The cytotoxity of the microcapsules increased with increasing mass concentration of the capsules. At the highest concentration of 0.12 mg/μL of the microcapsules, the cell viability was also maintained at about 87%. The results suggest that the microcapsules were low in toxicity with respect to the A549 cell line. By encapsulating the fluorescence dye molecules, RITC−PAH, into the microcapsules and incubating with A549 cells for 6 h, the dye-containing microcapsules were efficiently uptaken by the cells, and the emission of fluorescence molecules can be detected as shown in Figure 8b. This indicates that the $(Fe_3O_4/PAH)_4$ microcapsules could be rapidly attached or uptaken by the cell. The cell counting profile versus intensity of the green fluorescence is also given in Figure 8c, where the fluorescence intensity for the cells (FL1-H) with the microcapsules is much greater than that without microcapsules loading, agreeing well with those observed by confocal microscopy. These results indicate that cellular uptake of the $(Fe_3O_4/PAH)_4$ microcapsules can occur efficiently, and it is more interesting to expect that active molecules, for instance therapeutic drugs, can be efficiently released in a desirable manner through external magnetic stimulus after the microcapsules reside in the cells.

Conclusion

Magnetically responsive microcapsules comprising of Fe_3O_4 and PAH multilayer shell structure were prepared via a layer-by-layer colloid-templating technique. The use of fluorescence dye molecules allowed the shell structure as well as the microstructural evolution of the microcapsules to be monitored upon stimulation with the magnetic field. The microcapsules formed a nanocavity on the surface of the shell short after the magnetic field was applied; it is believed that continuous growth of the nanocavity caused surface cracks and finally led to rupture of the microcapsules upon a certain time period of magnetic stimulus. This microstructural evolution as a result of growing nanostructural defects correlated with the enhanced doxorubicin release profile while the field was applied, compared to the release profile without magnetic stimulus. However, a burstlike profile appeared when the field was applied to the microcapsules for a certain period of time, and this has been the result of microstructural evolution from crack growth to final rupture of the microcapsules. Such a magnetic-sensitive microcapsule permits a fast uptake by the A549 cancerous cell line and has been suggested to be an excellent anticancer drug carrier with a controllable drug release profile according to the degree of magnetically induced microstructural deterioration.

Supporting Information Available: Figures S1−S9. This material is available free of charge via the Internet at http://pubs.acs.org.

LA801138E

(52) Sukhorukov, G. B.; Rogach, A. L.; Zebli, B.; Liedl, T.; Skirtach, A. G.; Kchler, K.; Antipov, A. A.; Gaponik, N.; Susha, A. S.; Winterhalter, M.; Parak, W. J. *Small* **2005**, *1*, 194–200.

(53) De Geest, B. G.; Vandenbroucke, R. E.; Guenther, A. M.; Sukhorukov, G. B.; Hennink, W. E.; Sanders, N. N.; Demeester, J.; De Smedt, S. C. *Adv. Mater.* **2006**, *18*, 1005–1009.